

# Ultrasonic determination of real contact area of randomly rough surfaces in elastoplastic contact

A. Baltazar\*

*Instituto Tecnológico de Hermosillo, División de Estudios de Posgrado e Investigación  
Hermosillo, Sonora, México*

J.-Y. Kim

*Georgia Institute of Technology, George W. Woodruff School of Mechanical Engineering  
Atlanta, Georgia, U.S.A.*

S.I. Rokhlin

*The Ohio State University, Laboratory for Multiscale Materials Processing and Characterization,  
Edison Joining Technology Center Columbus, Ohio, U.S.A.*

Recibido el 15 de junio de 2005; aceptado el 12 de octubre de 2005

Micromechanical characterization of interfacial properties of non-conforming rough surfaces in contact was performed by a method based on ultrasonic waves. The method to estimate the interfacial properties is based on ultrasonic spectroscopy of signals reflected from the interface. Ultrasonic results are complemented with probabilistic contact mechanics to model the normal and tangential interfacial stiffness ( $K_N$  and  $K_T$ ) constants for different degrees of closure. The results show that a single set of stiffness constants  $K_N$  and  $K_T$  is sufficient to describe the dynamic response of the interface independently of the incident angle of the ultrasonic waves. Plastic deformation of the rough interface is studied using the same ultrasonic method. Experimental results indicate that the hysteretic effect observed by repetitive loading cycles is an indication of plastic deformation at the asperity summits with greater height values. The phenomenon is explained using micromechanical and probabilistic models. The results show the possibility of using the method to estimate the interfacial stiffness, presence of plastic deformation, and the real contact area, which in the past have been impossible to measure accurately.

*Keywords:* Interfacial stiffness; ultrasound; rough surfaces.

Caracterización micromecánica de propiedades interfaciales de superficies rugosas no-conformantes fue realizado mediante un método basado en ondas ultrasónicas. El método para estimar las propiedades interfaciales hace uso de espectroscopia ultrasónica de señales reflejadas desde la interfase. Resultados de las pruebas con ultrasonidos se complementan con análisis probabilístico y mecánica del contacto para modelar las constantes de rigidez normal y tangencial de ( $K_N$  y  $K_T$ ) para diferentes grados de acercamiento de las superficies. Los resultados muestran que un par único de constantes de rigidez  $K_N$  y  $K_T$  son suficientes para describir la respuesta dinámica de la interfase independientemente del ángulo de incidencia de la onda ultrasónica. Se estudió la deformación plástica de la interfase rugosa usando el mismo método ultrasónico. Los resultados experimentales indican que el efecto histerético observado durante la aplicación de cargas repetitivas es un indicador de la deformación plástica en las crestas de las asperezas con valores de alturas mayores. El fenómeno se explica usando modelos probabilísticos y micromecánicos. Los resultados muestran la posibilidad de usar el método para estimar el área de contacto real, el cual hasta ahora ha sido imposible de medir.

*Descriptores:* Rigidez interfacial; ultrasonido superficies rugosas.

PACS: 43.35.+d; 46.55.+d; 81.70.Cv

## 1. Introduction

The determination of interfacial properties for rough surfaces in mechanical contact is important in several realms of engineering. Processes such as friction, wear, lubrication, electrical and heat conduction on the micro and nano-scale involve a certain degree of contact. In all of these processes, it is essential to determine interfacial properties such as interfacial stiffness and real contact area, which depend on the condition of deformation at the interface. To understand the contacting problem, elastic, elastoplastic and plastic deformation processes need to be considered for the correct analysis of interference between rough surfaces.

In the past, ultrasound was used mainly for determination of defects and process and material characterization. However, techniques in the study of interface characterization

based on ultrasound propagation analysis have received limited emphasis, despite the fact that ultrasonic waves are insensitive to surface oxidation as the electrical resistance technique and it can be applied to non-metallic and opaque materials to which the electrical and optical techniques are not applicable.

Works have been reported on the study of ultrasonic wave interaction with imperfect interfaces formed by two non-conforming rough surfaces. For example, Kendall and Tabor (1971) experimentally studied the assessment of the real area of contact between two rough surfaces. Nagy (1992) and Margetan *et al.* (1992) describe the nature of interfacial imperfections in kissing and partial bonds using interfacial stiffness parameters. Drinkwater *et al.* (1997) described the link between the reflection coefficient and surface roughness

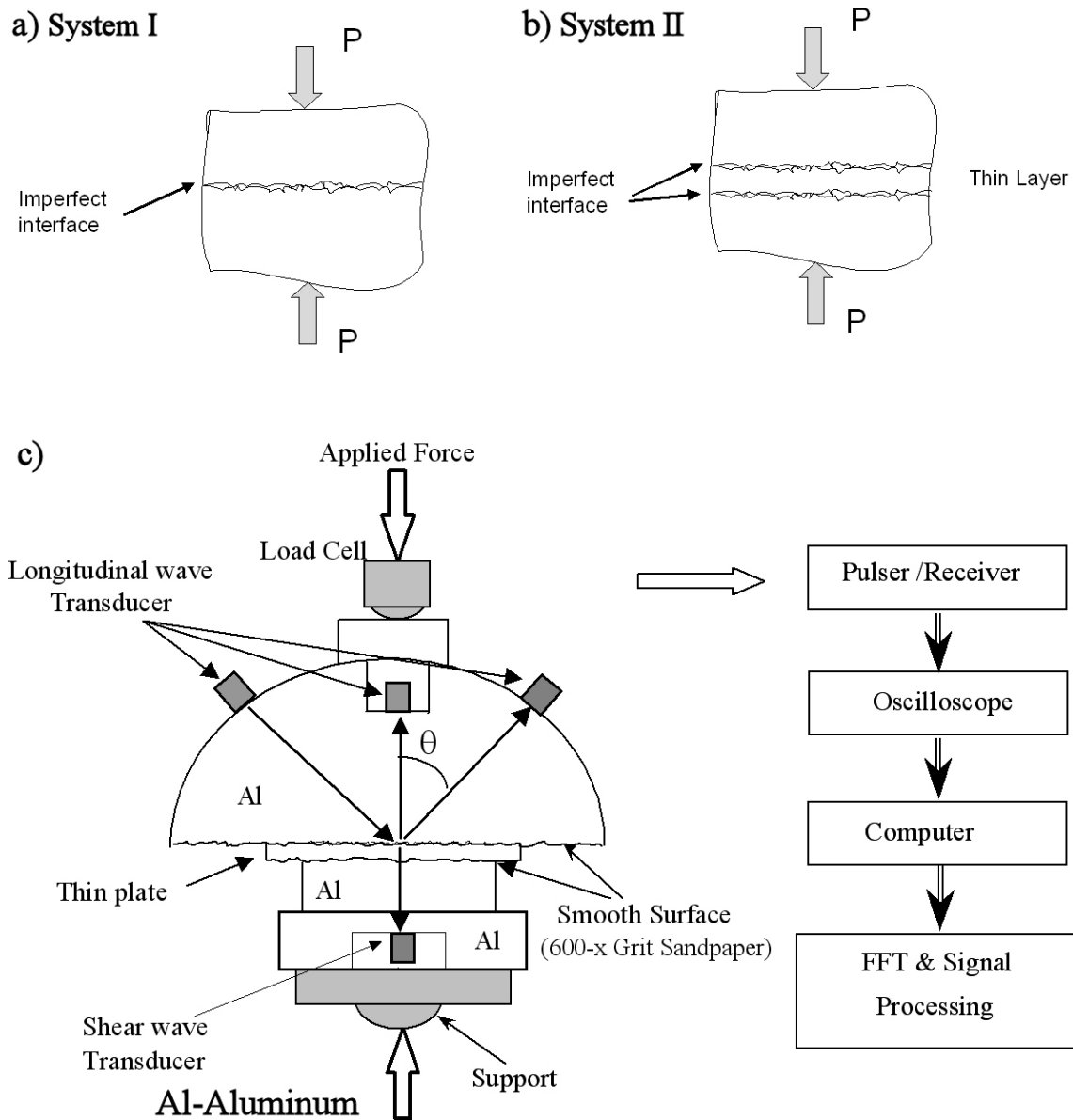


FIGURE 1. Studied systems (a) single interface, (b) double interface; (c) setup of the system and block diagram for signal acquisition and post processing for ultrasonic measurements of interfacial stiffness.

from an interface formed by rubber and a metal or plastic. Recently, the application of spectroscopic techniques to the study of imperfect interfaces was explored by Lavrentyev and Rokhlin (1998), Baltazar *et al.* (1999) and Baltazar *et al.* (2002). Kim *et al.* (2004) addressed the difference in the ultrasonically measured stiffness and static elastoplastic stiffness.

In this work, we addressed the use of ultrasonic spectrum signature in characterizing micromechanical properties, physical nature, including interfacial stiffness and real area of contact of two randomly rough metallic surfaces in close contact. The interfacial stiffness obtained with the ultrasonic method proposed is related to the micromechanical properties using developed probabilistic micromechanical models. Micromechanical models for elastic and elastoplastic regimes

are used in conjunction with the ultrasonically determined interfacial stiffness to extract the micromechanical properties of the interface. Finally, the possibility of extracting the area of contact from the ultrasonic spectrum signature for randomly rough interfaces with elastic and elastoplastic deformation is discussed.

## 2. Experimental determinations of interfacial stiffness using the ultrasonic method

### Quasi-Static Approach (QSA)

Ultrasonic determinations of interfacial stiffness were performed using nonlinear optimization between the experimental data and the Quasi-Static Approach (QSA) (Baik and

Thompson, 1984). In the QSA model, the low frequency response of two contacting surfaces causes a discontinuity in the displacement components ( $u_i$ ) that is proportional to the stress field ( $\sigma_{ik}$ ) at the interface, while for interfaces between contacting surfaces, the components of the stress fields are assumed to be continuous everywhere. When the characteristic length of the imperfection is sufficiently smaller than the wavelength, the stress and the displacement jump are related by the quasistatic (spring) boundary conditions. Thus, the spring boundary conditions enforced on the plane of an imperfect interface,  $z = 0$ , are:

$$\begin{aligned} \sigma_{zz}(z = 0^+) &= \sigma_{zz}(z = 0^-) \\ &= K_N [u_z(z = 0^+) - u_z(z = 0^-)], \\ \sigma_{xz}(z = 0^+) &= \sigma_{xz}(z = 0^-) \\ &= K_T [u_x(z = 0^+) - u_x(z = 0^-)], \end{aligned} \quad (1)$$

where  $z=0^+$  and  $z=0^-$  indicate above and below of the plane  $z=0$ . The quantities  $K_N$  and  $K_T$  ( $N/m^3$ ) are the normal and transverse interfacial stiffness constants of the imperfect interface, respectively.

**Experiments on single and double rough interface with elastic interference**

Experiments on rough interfaces were performed to model the elastic, elastoplastic and plastic contact of rough interfaces under controlled loading levels and correlated with micromechanical probabilistic models (Baltazar *et al.* 2002 and Kim *et al.* 2004). In the experiments, two different systems were considered: single interface (system I) and two rough interfaces (system II) as shown in Figs. 1a and 1b. System I consists of a single interface formed by two aluminum blocks in contact, and system II is formed by double interfaces composed of a thin aluminum plate placed between the two blocks. What interests us about these two systems is that both can be found in engineering structures, *i.e.* single interfaces are commonly found in mechanical structures in contact, and double interfaces can be found in joined systems such as adhesives.

The systems and the apparatus used in the experiments are described in Fig. 1c. In both cases, the systems were loaded against each other with different values of contacting surface roughness to control the interfacial stiffness. The applied pressure was varied from 9 to 80 MPa controlled by a universal testing machine (MTS). The upper block hosted three longitudinal wave transducers, one for normal incidence pulse-echo measurements and two for through-transmission oblique incidence (as shown in Fig. 1c). The transducers' signals were recorded using a digital oscilloscope and further analyzed in the time and frequency domain by a personal computer.

The aim in the first set of experiments was to observe if the set of interfacial stiffness constants are sufficient to characterize the macro-mechanical response of a system formed

by single or double imperfect interfaces independently of the angle of incidence of the incident ultrasonic beam. The effect of the applied load on the reflection spectrum was clearly observed, as shown in Fig. 2. Reconstruction of interfacial stiffness from the ultrasonic reflected spectra can be performed by least squares optimizing fit between the experimental spectrum and that calculated from the model. The average interfacial stiffness of the area illuminated by the ultrasonic beam is reconstructed (Baltazar *et al.* 2002).

Figure 2 shows typical results for an interface formed by two contacting rough surfaces (single interface), with 0.68  $\mu\text{m}$  rms roughness at each surfaces. The symbols represent the experimental values obtained at different values of the applied pressure, while the solid lines illustrate the predictions of the QSA model. For pressure values lower than 9 MPa applied to the system, the reflected ultrasonic amplitude does

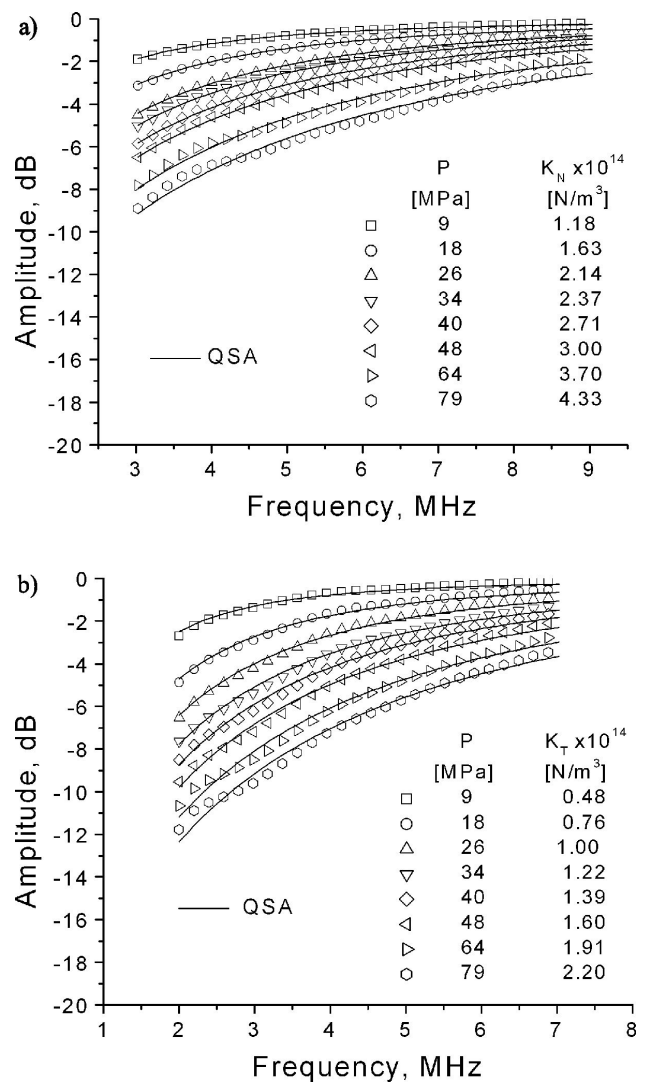


FIGURE 2. Experimental and theoretical spectra of a longitudinal wave at 9MPa, 34 MPa and 79MPa, for incidence at (a) normal and (b) 40 degrees of incidence from a double imperfect interface. The stiffness constants used in the model to calculate solid lines are those obtained at normal incidence.

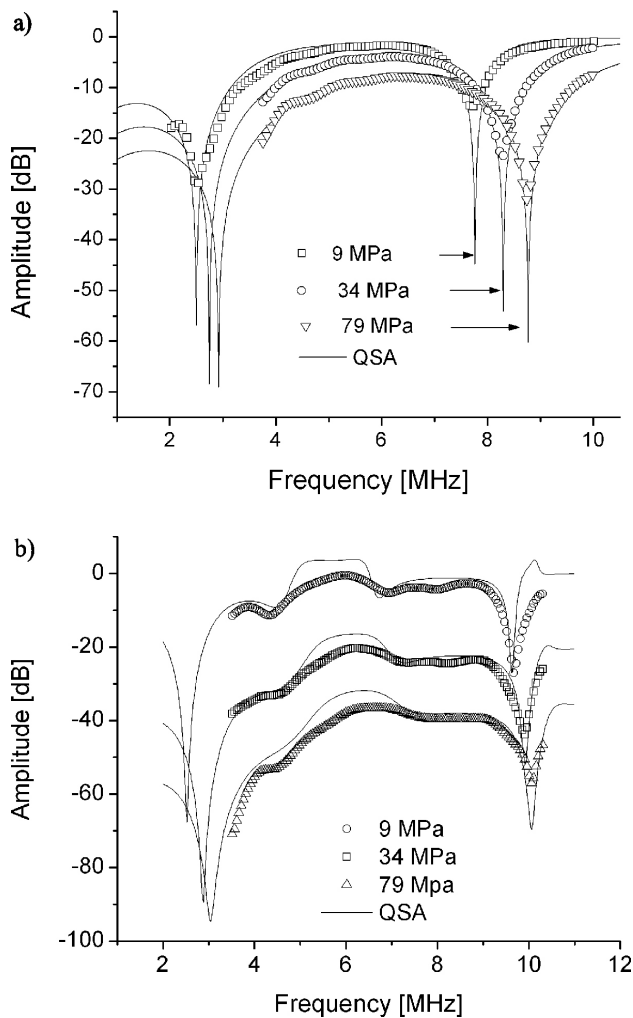


FIGURE 3. Experimental and theoretical spectra of a longitudinal wave at 9MPa, 34 MPa and 79MPa for incidence at (a) normal and (b) 40 degrees of incidence from a double imperfect interface. The stiffness constants used in the model to calculate solid lines are those obtained at normal incidence.

not vary with frequency, the interface behaves nearly as a perfectly reflecting surface, and the reflected ultrasonic amplitude does not vary with frequency. This pressure threshold varies with the roughness, being less for lower roughness. For values of the applied pressure higher than 80MPa, the effect of the contacts on the reflected spectra show signs of saturation, *i.e.* the reflection amplitude becomes independent of further load increase. Experiments were performed simultaneously using the shear wave to deduce the transverse stiffness constant.

To support our assertion that the stiffness constants obtained from single or double interfaces are the same, system II was investigated extending the work of Lavrentyev and Rokhlin (1998) on interfaces with imperfect boundary conditions to include oblique incidence, as in Baltazar *et al.* (2003). The interfacial stiffness of a double imperfect interface was evaluated from the normally reflected power spectra of both longitudinal and shear waves. The roughness of the

four surfaces used in these measurements was estimated to be about  $0.23 \mu\text{m}$ . The values of  $K_N$  and  $K_T$  obtained at normal incidence from a single interface (system I) were used to predict the spectral response of the double imperfect interface at oblique incidence.

Figures 3a,b shows an example of the measured and predicted spectra of a longitudinal wave reflected at 0 (normal incidence) and 40 degrees, respectively, from the double interface. The theoretical results reproduce the main features of the experimental spectrum and, in particular, correctly predict the position of the minima of the spectrum. Similar results were obtained for other values of the angle of incidence. The data provide evidence that for the given surfaces in contact there exists a unique set of transverse and longitudinal stiffness constants which describe sound wave interaction at an arbitrary incident angle.

The ratio between the transverse and the normal interfacial stiffness constants,  $K_T/K_N$ , increases from 0.4 at 9 MPa to 0.51 at 80 MPa, as shown in Fig. 4a. The data for longitudinal and shear stiffness for roughness  $\sigma = 0.25 \mu\text{m}$  are shown in Fig. 4b, together with the data for double interface. The small differences between  $K_N$  for a single and double interface are explained by the slightly different rms roughness values of the two surfaces and the different grade of aluminum for the thin foil used to form the double interface.

## 2.1. Hysteresis as an indicator of plastic deformation

In Figs. 5 and 6, repetitive loading cycling was investigated; this was done in a new set of experiments using ultrasonically measured normal interfacial stiffness versus applied nominal pressure. Experimental apparatus similar to that described in Fig. 1c was used; however, only normal incidence and single interface were considered. Ultrasonic measurements were performed on the rough surface contact interface; two

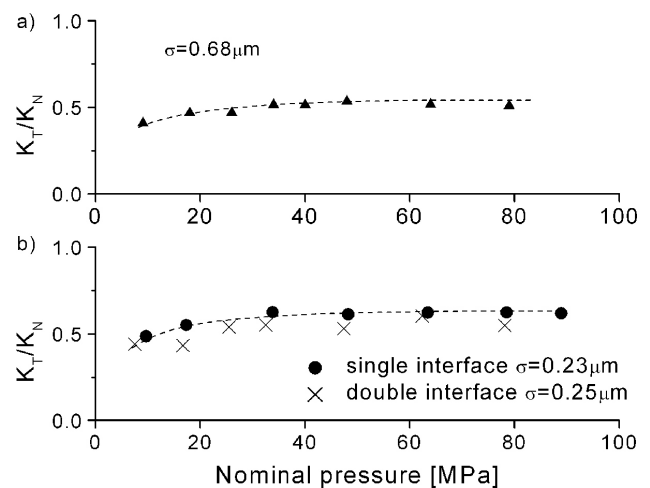


FIGURE 4. Ratio of experimental interfacial stiffness constants as function of nominal pressure. a) Single interface for surface roughness  $0.68 \mu\text{m}$ ; b) Comparative results for double interface (crosses) with *rms* roughness  $0.23 \mu\text{m}$  and results for single interface with roughness  $0.25 \mu\text{m}$  (solid points).

surface combinations for the upper and lower were used: 1) smooth/smooth surfaces, both surfaces having rms roughness of  $0.23 \mu\text{m}$ , obtained by sandpaper grinding (Fig. 5); 2) smooth/rough surfaces, the upper surface sandpaper-ground ( $0.23 \mu\text{m}$ ) and the bottom sandblasted ( $2.4 \mu\text{m}$ ) (Fig. 6). Measurements are shown by points for repeatable loading cycles. The stiffness data for the smooth/smooth interface (Fig. 5) exhibit very small hysteresis for the repeated cycles, indicating that the process is nearly elastic. Results for the smooth/rough interface are shown in Fig. 6, where a strong hysteretic behavior is clearly observed during the first cycle, which manifests the plastic deformation of the contacting asperities. The interfacial stiffness exhibits the same value at the maximum applied load of 85 MPa for all cycles, indicating that no further plastic deformation occurs at the asperities in subsequent loading cycles.

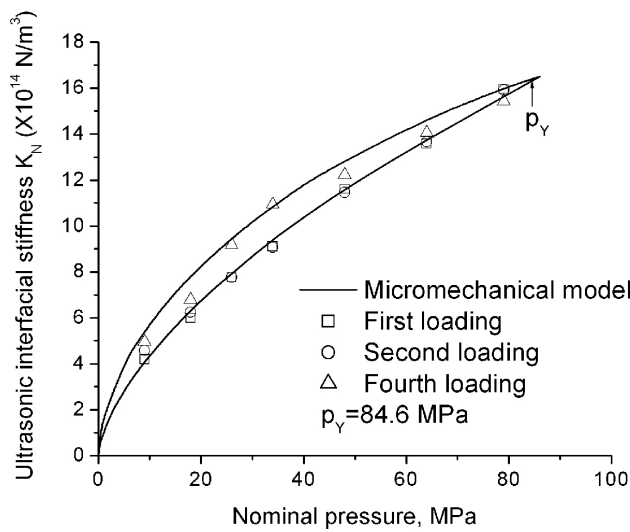


FIGURE 5. Interfacial stiffness versus nominal pressure. Points are experimental results. The solid lines correspond to the simulated hysteresis cycle.  $p_Y$  is determined from the model. Interface formed by two smooth surfaces with rms roughness  $0.25 \mu\text{m}$ .

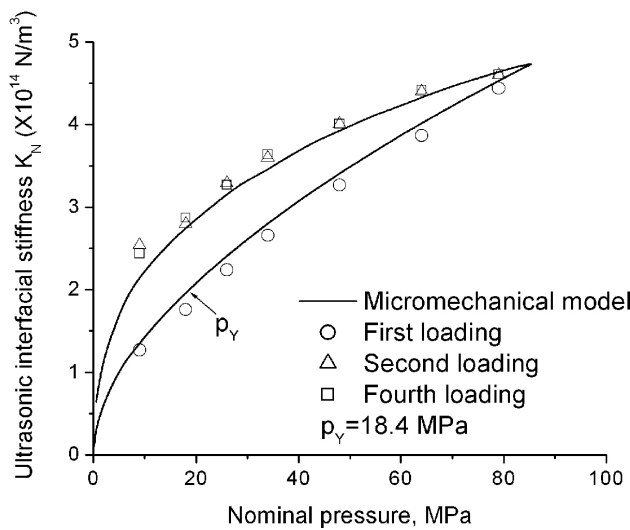


FIGURE 6. Interface formed by a rough (rms roughness  $2.4 \mu\text{m}$ ) and a smooth (rms roughness  $0.25 \mu\text{m}$ ) surface.

It should be noted that in the elasto-plastic regime, one must distinguish between the ultrasonically determined interfacial stiffness and static interfacial stiffness. As shown in Fig. 7, when an ultrasonic wave interacts with an interface, a small-scale loading-unloading cycle, centered on the static load, occurs (vibration displacement in an ultrasonic wave is of Åscale). In the elastic static contact regime, the ultrasonic loading-unloading occurs on the same static load-approach curve, and thus the ultrasonically determined interfacial stiffness corresponds to the static one as the slope of the load-displacement curve. When the contacting asperities are plastically deformed, the local unloading occurs along a curve different from the loading curve due to the hysteresis. The ultrasonic vibrations induce loading-unloading cycles along the local static unloading curve. Thus, the ultrasonically determined interfacial stiffness, which we call “ultrasonic interfacial stiffness,” is the local unloading stiffness.

In the elastoplastic and plastic contact regime, the ultrasonically determined interfacial stiffness is much higher than the static loading interfacial stiffness. This is because in the elastoplastic regime, the asperities have reduced their static stiffness with load due to progressive plastic deformation. Therefore, after an increase of load, the rate of static stiffness increase is less than that of the contact area. However, the ultrasonic stiffness corresponding to the local unloading slope is insensitive to the plastic softening effect of the asperities, and its increase is related solely to the contact radius growth as described in Fig. 6. This phenomenon is analogous to the recently described dynamic spring (stiffness) measurement in instrumented nano-indentation tests (Oliver and Pharr, 1992; Johnson, 1996; Cheng and Cheng, 1997; Fisher-Cripps, 2002). When a small oscillating load is applied during the indentation into the material, and calculating the unloading slope, Young’s modulus at the excitation frequency can be measured continuously during indentation.

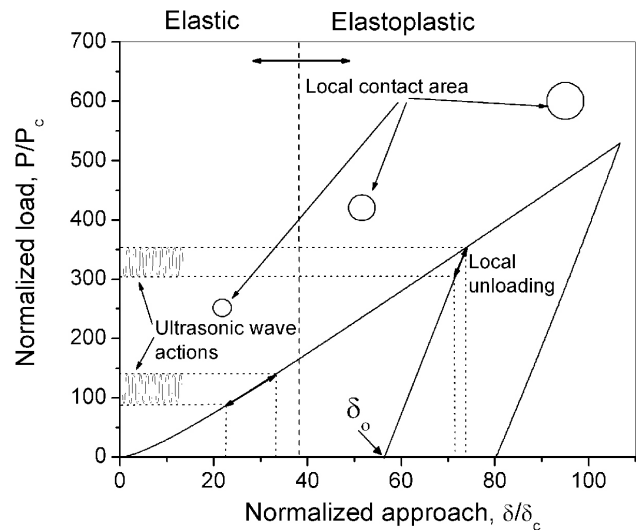


FIGURE 7. Diagram of pressure-approach loading-unloading cycle for a single asperity in elastoplastic contact. The relation between static and ultrasonic contact stiffness to the slope of the pressure-approach curve is shown.

While the question of the quantitative physical interpretation of this hysteresis continues to be under study, the above results indicate that the ultrasonically measured interfacial stiffness monitored during loading/unloading cycles is sensitive to the presence of plastic deformation. It also shows that an estimate of the contact area can be obtained from the estimated interfacial stiffness when data are used in conjunction with micromechanics models.

### 3. Micromechanical elastoplastic model

#### Ultrasonic contact spring

The problem of contact between rough interfaces is amenable to study using a single asperity model if non-interaction between neighboring asperities is assumed. The contact stiffness coefficient for a single asperity is defined from a force/displacement relation and has units N/m (Johnson, 1985), hereafter referred to as “contact spring coefficient” or “contact spring”. At any point of the loading curve (independently of the deformation extension), the contact spring ( $\kappa_l$ ) resulting from the ultrasonic vibrations is given by the slope of the initial unloading curve ( $dP_{unload}/d\delta$ ), which is calculated (Johnson, 1996) as:

$$\kappa_l = \frac{dP_{unload}}{d\delta} = 2aE^*, \quad (2)$$

where  $a$  is the elastoplastic radius of the contact area,  $\delta$  the relative approach,  $E^* = E/(1-\nu)$ .

Based on the FEM results of Kogut and Etsion (2002), a simple equation of the contact spring to describe the elastoplastic deformation for a single asperity can be determined. Therefore, the contact spring  $\kappa_l$  during loading is described in terms of the approach as (Kim *et al.*, 2004):

$$\kappa_l = 2CE^*a_c \left( \frac{\delta}{\delta_c} \right)^\lambda, \quad (3)$$

where  $C$  and  $\lambda$  are coefficients obtained for different ranges of the normalized approach ( $\delta/\delta_c$ ), and  $a_c$  and  $\delta_c$  are the radii of contact area and critical approach, respectively, at the yield inception as given by the Hertz theory (see Johnson, 1996).

The Hertz equations for the two spheres in elastic contact are recovered by setting  $C = 1$  and  $\lambda = 0.5$  for  $\delta/\delta_c \leq 1$ . In the range  $1 \leq \delta/\delta_c \leq 6$  (Kogut and Etsion (2002) found that the onset of plastic deformation is at  $\delta/\delta_c = 6$ ), the coefficients are  $C = 0.96$ ,  $\lambda = 0.568$ . In the elastoplastic range  $6 \leq \delta/\delta_c \leq 110$ , they are  $C = 0.97$  and  $\lambda = 0.573$ .

During unloading it can be assumed that Eq. 2 is still valid. However, the relationship between the displacement ( $\delta$ ) and the radius of contact area ( $a$ ) is generally unknown during the recovery from an arbitrary plastic state. In this work, we use the model proposed by Li *et al.* (2002) and early modified by Thornton (1997), where a truncated Hertzian contact pressure distribution is assumed over the contact area (assumption is supported by the recent analysis of Mesarovic and Johnson (2000)). An increase in the

radius of curvature is considered related to the radius of contact area using the parabolic law of the elastic contact problem,  $R = a^2/\delta$ . Therefore, the contact spring for the single asperity during unloading is given as:

$$\kappa_u = 2E^*(R_{\max}\delta)^{\frac{1}{2}}, \quad (4)$$

for  $\delta_r \leq \delta \leq \delta_{\max}$ . It is noted that at the initial point of unloading, the unloading contact spring coincides with the ultrasonic contact spring Eq. (3) at this point on the loading curve. The radius of contact area  $a$  during unloading is calculated by using the parabolic law  $a = \sqrt{R_{\max}\delta}$ , and thus the area of contact is  $A = \pi R_{\max}\delta$ .

Figure 8 compares the static and ultrasonic interfacial springs during loading and unloading. The ultrasonic contact spring during loading was calculated with Eq. (3), and the unloading contact spring with Eq. (4). The ultrasonic contact spring is continuous at the maximum load. The static loading contact spring was calculated as the slope of the load-displacement curve. Since the unloading is elastic, the static unloading spring is identical to the ultrasonic unloading spring. The ultrasonic unloading spring remains finite at load removal, which corresponds to the infinitely small load at the residual displacement. One can see that the ultrasonic stiffness at a given load depends only on the contact area, which remains unchanged at the initial unloading point.

#### Interfacial stiffness

The single asperity model discussed in the previous section is now extended to cover the problem of estimating the interfacial stiffness of a rough interface in mechanical contact with elastic-plastic deformation.

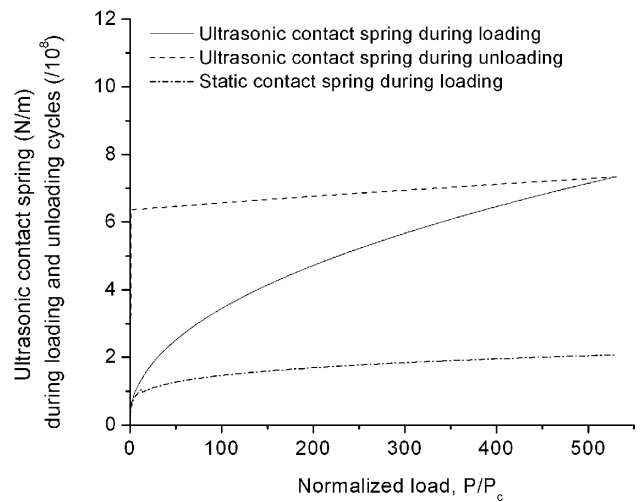


FIGURE 8. Ultrasonic contact spring during loading and unloading of two identical spheres in contact. The static contact spring ( $dP_{load}/d\delta$ ) is also shown (dash-dotted line); the locus for the static unloading contact spring coincides with that for the ultrasonic unloading spring.

Most of the micromechanical non-interacting models in the past assume that deformation occurs at the surface asperities, and their interaction is to be purely elastic (Kendall and Tabor (1971), Brown and Scholz (1985), Boitnott *et al.* (1992), Yoshioka and Scholz (1989)). Significant efforts have been put forth by many authors to model elastoplastic behaviors of rough surfaces, *e.g.* Haines (1980), Nayak (1973), Webster and Sayles (1986), and Yoshioka (1994). Models for contacting rough surfaces based on improved elastoplastic descriptions of the two-spheres contact problem have been proposed (Chang *et al.*, 1987; Zhao *et al.*, 2000). Recently, theoretical and finite element analyses (FEA) of the elastoplastic contact behavior of two spheres during loading cycles have been reported by Vu-Quoc and Zhang (1999), Mesarovic and Johnson (2000), Mesarovic and Fleck (2000) and Li *et al.* (2002). Kogut and Etsion (2002) performed detailed FEA elastoplastic analysis of spheres in contact and based on the FEA results, provided empirical coefficients of dimensionless relations for load, real area of contact, and contact pressure versus relative approach.

The topography of two contacting rough surfaces plays a significant role in the ultrasonic interaction model. In the past, several stochastic models have been used to describe rough surfaces.

To simplify the problem of two rough surfaces in contact, Greenwood and Williamson (1966) described the statistical asperity micromechanical model where the properties of the two rough surfaces are accounted for through the statistical properties of the fictitious composite surface. Therefore the new surface is defined by means of an appropriate algebraic sum of the profiles of the two contacting surfaces. In this way, the contact of the real rough surfaces is transformed into that of the composite surface in contact with a rigid flat surface.

The distribution of the peaks of the asperity heights of the composite surfaces can be described statistically by a probability density function  $\varphi(z)$ . This function defines the probability of finding peaks of asperity heights in the interval  $dz$  around  $z$ . The probability density function is therefore a key element to describing the contacting problem. Two major difficulties arise in correctly defining this function: the first is related to the nature of the roughness preparation, and the second related to the method used to estimate the surface topography. In nature, most surface topography is formed by a random distribution of surface height which can be classified as either Gaussian (*i.e.* Greenwood and Williamson, 1966) or non-Gaussian (Goodman (1976), Adler and Firman (1981), Aronowich and Adler (1995), Chilamakuri and Bhushan, 1998) depending on the surface preparation method used. For example, surfaces produced by common machine methods are expected to have a non-Gaussian height distribution. Skewness in the distribution is common in surfaces obtained by processes such as grinding, honing, milling and abrasion (Bhushan, 2001). Typically, the surface statistics are estimated using a profile measuring instrument. These measurements are limited by the inability of the device to move along the summit of the asperities; instead, the device

is expected to travel along the shoulder of the asperity. Studies based on random process theory showed that the statistics profiles are close to the actual summit distribution when this resembles wide-band random noise, rich in frequency components. To account for this, Nayak (1971) defined a bandwidth parameter  $\alpha$ . Analysis of Gaussian (Nayak, 1971) and non-Gaussian (Aronowich and Adler, 1985) height distributions showed similar shifting of the summit distribution to the greater height values as the bandwidth parameter  $\alpha$  decreases. Bush *et al.* (1976) described the following approximation for the rms of the summit or peaks as function of  $\alpha$  and the rms of the profile  $\sigma'$ :

$$\sigma = \left(1 - \frac{0.8968}{\alpha}\right)^{1/2} \sigma'. \quad (5)$$

To account for the skewness and kurtosis of the probability density function, Chilamakuri and Bhushan (1998) generated non-Gaussian probability density distributions for different values of skewness and kurtosis values. Adler and Firman (1981) proposed using an inverted chi-squared distribution; this approach was later corrected by Aronowich and Adler (1985). In this present work, we have proposed the use of the following simpler distribution function which is a limiting case of that derived by Aronowich and Adler (1985) when the values of the parameter  $\alpha \rightarrow \infty$  (Baltazar *et al.*, 2002):

$$\varphi(\beta; z) = \sqrt{\frac{\beta}{2}} \frac{1}{\sigma} \frac{\left(\sqrt{\frac{\beta}{2}} \frac{z}{\sigma}\right)^{\frac{\beta-2}{2}}}{\Gamma\left(\frac{\beta}{2}\right)} \exp\left(-\sqrt{\frac{\beta}{2}} \frac{z}{\sigma}\right), \quad (6)$$

where  $\sigma$  is the rms roughness value of the composite surface profile defined as  $\sigma = [\sigma_1^2 + \sigma_2^2]^{1/2}$ ,  $\sigma_{1,2}$  are the rms roughness values of the two surfaces, and  $z$  is the coordinate attached at the top of the highest asperity with its positive direction coincident with the depth direction as shown in Fig. 9a. Since the distribution of heights of asperity peaks is unknown and to be determined from the ultrasonically measured elastoplastic response of the interface, the use of the  $\chi^2$ -distribution function is advantageous due to its generality. In limiting cases it becomes the exponential distribution at  $\beta \leq 2$  and the Gaussian distribution at  $\beta \rightarrow \infty$ .

Using the composite surface and the probability density function for peaks of asperity heights, the total ultrasonic contact spring  $\bar{\kappa}$  can be expressed as a function of the approach as

$$\bar{\kappa}(\delta) = \eta A_n \int_0^{\delta} \kappa(\delta - z) \varphi(z) dz, \quad (7)$$

where  $\eta$  is the number of asperities per unit area; the overbar denotes the statistical average of a random physical quantity,  $A_n$  is the nominal contact area,  $(\delta - z)$  is the deformation of a given asperity at approach  $\delta$ , and  $\kappa(\delta - z)$  is the contact spring of a single spherical asperity.

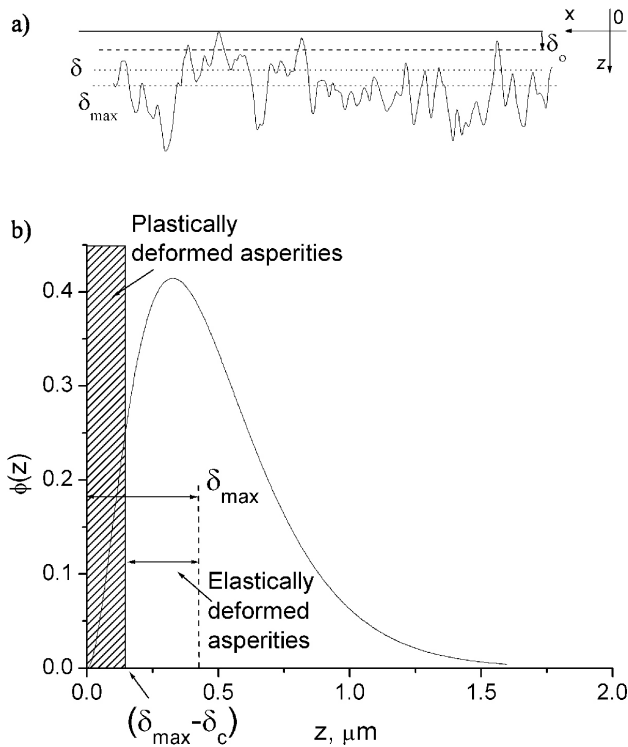


FIGURE 9. (a) Diagram showing coordinate system; (b) Asperity height distribution function. The ranges of approach in which asperities are deformed plastically and remain elastic are shown. All asperities with height below  $\delta_{max} - \delta_c$  ( $z < \delta_{max} - \delta_c$ ) are deformed elastically while asperities with height above this line are deformed elastoplastically.

The total real contact area can then be found as

$$\bar{A}(\delta) = \eta A_n \int_0^{\delta} A(\delta - z) \varphi(z) dz, \quad (8)$$

where  $A(\delta - z)$  are the corresponding functions for the contact of a single spherical asperity.

After substituting Eqs. (3) and (6) into Eqs. (7) and (8) and normalizing them appropriately, the ultrasonic stiffness of the interface during loading and unloading can be obtained as

$$\frac{\bar{K}_l(\delta')}{E^* / \sigma} = 2C\gamma R_o'^{-1} a_c'^2 \delta_c'^{-2\lambda} \int_0^{\delta'} (\delta' - z')^\lambda \varphi^*(\beta; z') dz', \quad (9)$$

and from Eqs. (3) and (8) the actual area of contact is:

$$\frac{\bar{A}(\delta')}{A_n} = \pi C^2 \gamma R_o'^{-1} a_c'^2 \delta_c'^{-2\lambda} \int_0^{\delta'} (\delta' - z')^{2\lambda} \varphi^*(\beta; z') dz', \quad (10)$$

where  $\gamma = R_o' \eta \sigma^2$  is the nondimensional parameter depending only on the rough surface properties; the prime denotes normalization of the length scale by the  $\sigma g$  rms roughness of the composite surface, e.g.  $R_o' = R_o / \sigma$  and  $z' = z / \sigma$ . The three independent parameters ( $\sigma / R_o$ ,  $\gamma$ ,  $\beta g$ ) can be estimated from the ultrasonic stiffness measurements during the

loading-unloading cycle. These parameters are necessary to compute the actual area of contact as functions of the approach from Eqs. (10).

The interfacial stiffness during unloading is calculated using Eq. (4) for a single asperity. The final curvature radius  $R_{max}$  of asperities with different heights  $z$  is calculated using Eq. (3) with  $R_{max} = R(z_{max})$ . The residual deformation  $\delta_r(z)$  is calculated also as a function of  $z$  using Eq. (10) for a given maximum approach  $\delta_{max}$ . Therefore, at the end of the loading, all parameters of plastically deformed asperities are known as a function of their initial heights  $z$  in the distribution (10).

Since the unloading is elastic, the interfacial stiffness and the area of contact are calculated as

$$\frac{\bar{K}_u(\delta')}{E^* / \sigma} = 2\gamma R_o'^{-1} \times \int_{\delta'_o}^{\delta'} R_{max}'^{1/2}(z') (\delta' - z')^{1/2} \varphi^*(\beta; z') dz', \quad (11)$$

$$\frac{\bar{A}_u(\delta')}{A_n} = \pi\gamma R_o'^{-1} \times \int_{\delta'_o}^{\delta'} R_{max}'(z') (\delta' - z') \varphi^*(\beta; z') dz'. \quad (12)$$

In integrals (11) and (12),  $\delta'$  is between and  $\delta'_{max}$ . The integration considers all load bearing asperities during unloading. As shown in Fig. 8b, those asperities are elastically or plastically deformed if  $\delta'_{max} - \delta'_c < \delta' < \delta'_{max}$ , they are all plastically deformed when  $\delta'_{max} - \delta'_c > \delta'$ . At a given  $\delta'$ , we include in the calculations only those plastically deformed asperities with original summit heights in the range whose heights remain in that range after the load is relieved; otherwise they are not load-bearing asperities (the undeformed height of the asperity  $z$  from distribution in Eq. (10) may be in the range; however, after deformation it is residually deformed and its  $z'$  may be larger than (height is reduced) and be outside this range, Fig. 9b).

Figure 10 shows calculated loading-unloading cycles describing the detailed history of elastoplastic deformation at the interface under consideration. Upon load removal, the ultrasonic stiffness values of the rough interfaces are reduced to zero. When the many asperities of the rough surface are in contact, the unloading process occurs gradually due to distribution of the asperity heights. With load removal, fewer and fewer asperities are in contact and load-bearing. At a negligibly small load, only a few (the number depends on the height distribution) of the numerous asperities remain in contact, resulting in remote contact stiffness. In fact, this process is described in our model excluding the asperities that are not in contact.

TABLE I. Mechanical properties of the aluminum 6061-T6 alloy samples.

Property	Value
Young's modulus, $E$	71.0 GPa
Hardness, $H_B$	94
Yield stress, $\sigma_Y$	235 MPa
Poisson's ratio, $\nu$	0.33
rms surface roughness, $\sigma$	0.23 and 2.4 $\mu\text{m}$
Nominal contact area, $A_n$	5.06 $\text{cm}^2$

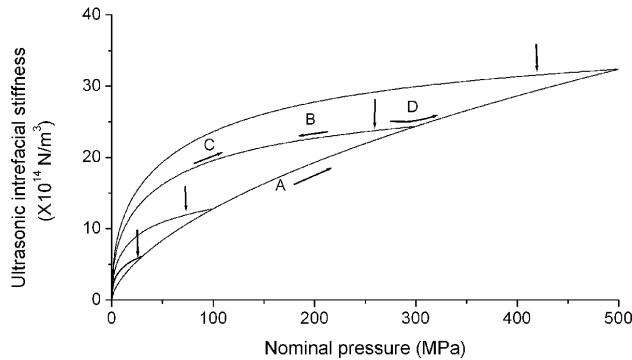


FIGURE 10. Ultrasonic interfacial stiffness versus nominal pressure during loading and unloading cycles with increasing maximum cycle load. The parameters in the calculation are  $\sigma/R = 1.92 \times 10^{-3}$ ,  $n=2$  and  $\sigma = 3.5 \mu\text{m}$ , Young's modulus  $E=69$  GPa, Poisson's ratio  $\nu=0.33$ , yield stress  $\sigma_Y = 235$  MPa and plasticity index  $\psi=5.1$ .

Increased hysteresis is observed for cycles at higher loads due to an increasing plastic flow. The loading-unloading path for the third cycle is labeled in Fig. 10. Since the unloading is assumed to be elastic, the reloading curve (C) coincides with the unloading curve (B) in the second cycle. The path for loading (D) beyond the previous maximum load follows the original loading curve path. It is also observed that the slope of the interfacial ultrasonic stiffness at the initial stage of unloading (marked in Fig. 10 by arrows) decreases with increasing maximum load in the cycle (from the first to the fourth hysteresis loop). This indicates an increasing conformity between the two surfaces with the increase of maximum load due to the significant plastic flow accumulated during loading so that the area of contact (and the unloading curve slope) changes very little during the initial stage of unloading. Similar hysteretic behavior has been observed experimentally by Dwyer-Joyce *et al.* (2001).

In Fig. 3, the calculated ultrasonic dynamic interfacial stiffness for loading-unloading cycles is shown by solid lines, along with those measured for three different surface combinations: smooth-smooth (Fig. 3a) and rough-smooth (Fig. 3b). The pressures at the onset of plastic deformation ( $p_Y$ ) for the tallest asperities at  $z=0$  are indicated. The theoretical curves were obtained using the material and surface properties listed in Table I. The nondimensional parameters

TABLE II. Model parameters.

Surface	Given	Reconstructed		Calculated using reconstructed parameters		
	$\sigma^1$ ( $\mu\text{m}$ )	$\mu/R$	$\gamma$	$\beta$	$\psi$	$p_Y$ (MPa)
Smooth-smooth	0.325	$2.01 \times 10^{-4}$	2.4	3.0	1.63	84.6
Rough-smooth	2.4	$1.20 \times 10^{-3}$	2.62	1.5	4.01	18.4

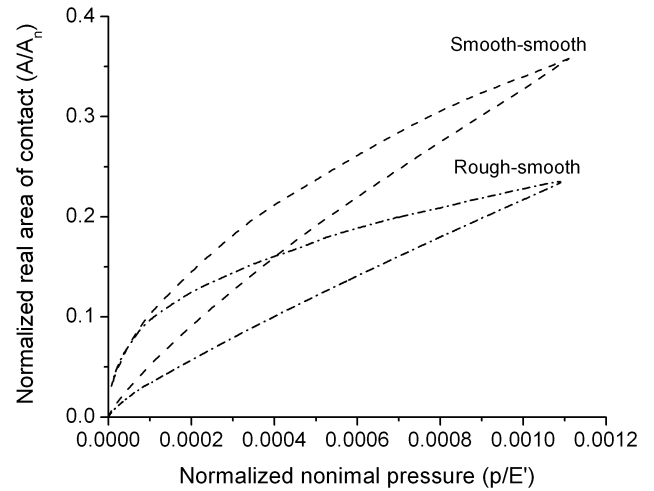


FIGURE 11. Normalized real area of contact versus normalized nominal pressure for smooth-smooth ( $\psi=1.63$ ;  $\sigma=0.325 \mu\text{m}$ ), rough-smooth ( $\psi=4.01$ ;  $\sigma=2.4 \mu\text{m}$ ), rough-rough ( $\psi=5.12$ ;  $\sigma=3.4 \mu\text{m}$ ) surfaces; calculated using the surface parameters reconstructed from experimental data (Table II).

$\gamma$ ,  $R'_o$  and  $\beta$  were found by the nonlinear least square optimization (Baltazar *et al.*, 2002) between experimental data  $K_i^{Exp}$  and model computations  $K_i^{Theory}$ .

The interface between two smooth surfaces exhibits a nearly elastic behavior with very small hysteresis, as shown in Fig. 3. The onset of plastic deformation occurs at almost the maximum applied pressure,  $p_Y=84.6$  MPa. The other interface (Fig. 6) exhibits elastoplastic behaviors with higher levels of hysteresis. The reconstructed parameters show increasing levels of plasticity with the increase of rms roughness. For example, the plasticity index for the rough-rough interface is highest, and that for the smooth-smooth interface is lowest. For rough aluminum surfaces, the elastoplastic behavior occurs when  $\psi > 1$  (Huchings, 1992). Our results agree with this observation. The parameter  $\beta$  for the smooth-smooth interface ( $\beta=3$ ) is close to those obtained in our previous work for the elastic contact of smooth interfaces (Baltazar, 2002). In contrast, those for the rough-smooth interface are relatively small ( $\beta \leq 2$ ), leading to nearly exponential type distribution functions, which implies that the asperity summits are densely populated near the sample surface ( $z=0$ ). Since the ultrasonic measurements of interfacial stiffness for these interfaces are taken mostly in the elastoplastic region (at loads higher than  $p_Y$  of the interface), the ultrasonic wave

first probes the interfaces after the highest summits are already plastically deformed so that the surface is effectively flatter than the initial surface. Moreover, the unloading starts with the interface asperities further flattened due to loading, thus producing even smaller values of  $\beta$ . The smallest value of  $\beta$  for the smooth-rough case reflects the appearance of the observed results on the smooth surface indentations of the rough surface asperities. This improves the “fit” between the surfaces, which corresponds to the equivalent flattening of composite surface asperities and therefore decreases  $\beta$ .

The real area of contact is therefore estimated by applying the statistical elastoplastic contact model to the ultrasonically measured interfacial stiffness, and determining the necessary unknown parameters: the asperity number density and the vertical distribution of the asperities related to the parameter  $\beta$ . This produces the minimal sufficient set of parameters needed to compute the real area of contact.

Figure 11 shows the real area of contact normalized with the apparent contact area versus the normalized pressure for the two interfaces considered in our experiments (Figs. 5 and 6). It is noted that the real area of contact increases nearly linearly with the load, especially in the region of the elastoplastic deformation (this was experimentally observed by Greenwood and Williamson, 1966), whereas unloading behavior is nonlinear with very sharp decreases to zero of the contact area with the load removal.

## 4. Summary

An ultrasonic spectroscopy method combined with an elastoplastic contact model for determining of interface properties that can be related to the real area of contact was discussed. In the present work, we have demonstrated the feasibility of predicting the real area of contact. This is done by applying the statistical elastoplastic contact model to the ultrasonically measured interfacial stiffness and determining the unknown necessary parameters: the asperity number density and the vertical distribution of the asperities related to the parameter  $\beta$ . This produces the minimal sufficient set of parameters needed to compute the real area of contact. Data from ultrasonic measurements were reported during loading-unloading static cycles on different interface conditions formed by aluminum surfaces with different levels of roughness. From the ultrasonic reflection spectra measured, the interfacial stiffness constants were calculated. The experimentally measured hysteresis observed during loading-unloading cycles is attributed to plastic deformation at the tips of the asperities. To explain the ultrasonically-measured stiffness of rough surfaces in elastoplastic contact, the dynamic stiffness, which should be distinguished from static loading stiffness, is introduced. An elastoplastic micromechanical asperity contact model is proposed to describe the mechanical hysteresis during the loading and unloading cycles. The micromechanical model allows us to demonstrate the elastoplastic histories during the loading-unloading cycles.

\* Corresponding author.

1. R.J. Adler and D. Firman, *Philos. Trans. R. Soc. London. Ser. A* **303** (1981) 433.
2. M. Aronowich and R.J. Adler, *Adv. Appl. Prob.* **17** (1985) 280.
3. J.M. Baik and R.B. Thompson, *J. Non-Destruct. Eval.* **4** (1984) 177.
4. A. Baltazar, S.I. Rokhlin, and C. Pecorari, On the Relationship Between Ultrasonic and Micro-structural Properties of Imperfect Interfaces in Layered Solids, in *Review of Progress in Quantitative Nondestructive Evaluation*, D.O. Thompson and D.E. Chimenti, eds. (American Institute of Physics, New York, 1999) Vol. 18B p. 1463.
5. A. Baltazar, S.I. Rokhlin, and C. Pecorari, *J. Mech. Phys. Solids* **50** (2002) 1397.
6. A. Baltazar, L. Wang, B. Xie, and S.I. Rokhlin, *The Journal of the Acoustical Society of America* **114** (2003) 424.
7. B. Bhushan, *Modern tribology handbook* (CRC Press LLC, 2001).
8. G.N. Boitnott, R.L. Biegel, C.H. Scholz, N. Yoshioka, and W. Wang, *J. Geoph. Res.* **97** (1992) 8965.
9. S.R. Brown and C.H. Sholtz, *J. Geophys. Res.* **90** 1985 5531.
10. A.W. Bush, R.D. Gibson, and G.P. Keogh, *Mech. Res. Commun.* **3** (1976) 169.
11. W.R. Chang, I. Etsion, and D.B. Bogy, *ASME J. Tribol* **109** (1987) 257.
12. C.-M. Cheng and Y.-T. Cheng, *Appl. Phys. Lett.* **71** (1997) 2623.
13. S.K. Chilamakuri and B. Bhushan, *Proc. Inst. Mech. Eng. Part J: J. Eng. Tribol* **212** (1998) 19.
14. B. Drinkwater, R. Dwyer-Joyce, and P. Cawley, *J. Acoust. Soc. Am.* **101** (1997) 970.
15. R.S. Dwyer-Joyce, B.W. Drinkwater, and A.M. Quinn, *ASME Trans. J. Tribol.* **123** (2001) 8.
16. A.C. Fisher-Cripps, *Nanoindentation* (Springer, New York, 2002).
17. R.E. Goodman, “Methods of Geological Engineering” in (Discontinuous Rocks, West Publishing, New York, 1976).
18. J.A. Greenwood and J. Williamson, *Proc. R. Soc., London, Ser. A* **295** (1966) 300.
19. Haines, N. F., 1980. The theory of sound transmission and reflection at contacting surfaces, CEGB Report RD-B-N4744, Berkeley Nuclear Laboratories.
20. I.M. Huchings, *Tribology; Friction and wear of engineering materials* (St. Edmundsbury Press, Cornwell, 1992).
21. Johnson, K. L., *Contact mechanics*. Cambridge University Press, Cambridge, 1985.

22. K.L. Johnson, Modelling the indentation hardness of solids. Proceedings of the First Royal Society-Unilevel Indo-Uk Forum in material Science and Engineering, Solid-Solid interactions (Imperial College Press, 1996) p. 16.
23. K. Kendall and D. Tabor, *Proc. Roy. Soc. Lond. A* **323** (1971) 321.
24. J.-Y. Kim, A. Baltazar, and S.I. Rokhlin, *J. Mech. Phys. Solids* **52** (2000) 1911-1934.
25. Kogut, and I. Etsion, *J. Appl. Mech.* 69 (2002) 657.
26. A.I. Lavrentyev and S.I. Rokhlin, *J. Acoust. Soc. Am.* **103** (1998) 657.
27. L.-Y. Li, C.-Y. Wu, and C. Thornton, *Proc. Instn. Mech. Engrs. C* **216** (2002) 421.
28. F.J. Margetan, R.B. Thompson, J.H. Rose, and T.A. Gray, *J. Non-Destruct. Eval.* **11** (1992) 109.
29. S. Dj. Mesarovic and K.L. Johnson, *J. Mech. Phys. Solids* **48** (2000) 2009.
30. Mesarovic, S. Dj., Fleck, N.A., 2000. Frictionless indentation of elastic-plastic solids. *Int. J. Solids Struct.* 37, 7071-7091.
31. P.B. Nagy, *J. Non-Destruct. Eval.* **11** (1992) 127.
32. P. Nayak, *J. Lubr. Tech.* **93** (1971) 398.
33. P.R. Nayak, *Wear* **25** (1973) 305.
34. W.C. Oliver and G.M. Pharr, *J. Mater. Res.* **7** (1992) 1564.
35. C. Thornton, *J. Appl. Mech.* **64** (1997) 383.
36. L. Vu-Quoc and X. Zhang, *Proc. R. Soc. (Lond) A* **455** (1999) 4013.
37. M. Webster and R.S. Sayles, *Trans. ASME-J. Tribol.* **108** (1986) 314.
38. N. Yoshioka, *J. Geophys. Res. B* **99** (1994) 15561.
39. N. Yoshioka and C.H. Scholz, *Theory. J. Geophys. Res.* **94** (1989) 17681.
40. D. Zhao, M. Maietta, and L. Chang, *J. Tribol. ASME* **122** (2000) 86.